

RESEARCH LETTER

10.1029/2018GL079706

Key Points:

- Basal glacial meltwater beneath an ice shelf is quantified for the first time with helium and neon samples
- Inside the ice shelf cavity, meltwater fractions up to 3.6% were measured
- Up to 2.7% of the meltwater had refrozen, and we identified a local source of crustal helium

Supporting Information:

- Supporting Information S1

Correspondence to:

O. Huhn,
 ohuhn@uni-bremen.de

Citation:

Huhn, O., Hattermann, T., Davis, P. E. D., Dunker, E., Hellmer, H. H., Nicholls, K. W., et al. (2018). Basal melt and freezing rates from first noble gas samples beneath an ice shelf. *Geophysical Research Letters*, 45, 8455–8461. <https://doi.org/10.1029/2018GL079706>

Received 23 JUL 2018

Accepted 31 JUL 2018




Accepted article online 6 AUG 2018

Published online 28 AUG 2018

©2018. The Authors.

This is an open access article under the terms of the Creative Commons Attribution-NonCommercial-NoDerivs License, which permits use and distribution in any medium, provided the original work is properly cited, the use is non-commercial and no modifications or adaptations are made.

Basal Melt and Freezing Rates From First Noble Gas Samples Beneath an Ice Shelf

Oliver Huhn^{1,2} , Tore Hattermann² , Peter E. D. Davis³ , Erich Dunker², Hartmut H. Hellmer² , Keith W. Nicholls³ , Svein Østerhus⁴, Monika Rhein^{1,5} , Michael Schröder², and Jürgen Sültenfuß¹ 

¹Institute for Environmental Physics IUP, Oceanography Department, University of Bremen, Bremen, Germany, ²Alfred Wegener Institute, Helmholtz Centre for Polar and Marine Research, Bremerhaven, Germany, ³British Antarctic Survey, Cambridge, UK, ⁴Uni Research Climate, Bergen, Norway, ⁵Center for Marine Environmental Sciences MARUM, University of Bremen, Bremen, Germany

Abstract A climatically induced acceleration in ocean-driven melting of Antarctic ice shelves would have consequences for both the discharge of continental ice into the ocean and thus global sea level, and for the formation of Antarctic Bottom Water and the oceanic meridional overturning circulation. Using a novel gas-tight in situ water sampler, noble gas samples have been collected from six locations beneath the Filchner Ice Shelf, the first such samples from beneath an Antarctic ice shelf. Helium and neon are uniquely suited as tracers of glacial meltwater in the ocean. Basal meltwater fractions range from 3.6% near the ice shelf base to 0.5% near the sea floor, with distinct regional differences. We estimate an average basal melt rate for the Filchner-Ronne Ice Shelf of 177 ± 95 Gt/year, independently confirming previous results. We calculate that up to 2.7% of the meltwater has been refrozen, and we identify a local source of crustal helium.

1. Introduction

In recent decades, volume loss from ice shelves, the floating extensions of the Antarctic ice sheet, has accelerated, especially in West Antarctica (Paolo et al., 2015; Shepherd et al., 2018). Filchner-Ronne Ice Shelf (FRIS), located in the southern Weddell Sea, is the largest ice shelf by volume. At present, its rate of thickness change shows large pentadal variability, with the highest thickness losses in more recent years (Paolo et al., 2015). Freezing beneath some areas of FRIS has also been observed (Rignot et al., 2013). Over the coming century, climatically induced increases in mass loss due to submarine (basal) melting have been predicted, driven by warmer water of circumpolar origin intruding into the cavity below FRIS (Hellmer et al., 2012; Timmermann & Hellmer, 2013). Increased basal melting will thin the ice shelf, reducing buttressing and allowing grounded ice to flow into the ocean at a greater rate, with consequences for the global sea level (Bamber et al., 2009; Shepherd et al., 2012). Ice shelf-ocean interactions are also important for the formation of Antarctic Bottom Water, modifying the properties of the deepest limb of the global overturning circulation (Foldvik et al., 1985).

Most contemporary estimates of ice shelf melt and refreezing rates are based on remote sensing and/or modeling approaches (Hellmer, 2004; Paolo et al., 2015; Rignot et al., 2013; Schodlok et al., 2016; Timmermann & Hellmer, 2013), observations of heat and salt budgets combined with ice data and numerical models (Jacobs et al., 2011; Nicholls et al., 2001, 2006; Nicholls & Makinson, 1998; Nicholls & Østerhus, 2004; Nicholls et al., 2009), or phase-sensitive radar systems, *pRES* (Corr et al., 2002). While measurements of helium isotope He (henceforth He) and neon isotopes Ne (henceforth Ne) is a powerful tool that can detect the presence of basal meltwater in the ocean (Aeschbach, 2016; Hohmann et al., 2002; Huhn et al., 2008; Schlosser, 1986; Schlosser et al., 1990; Weppernig et al., 1996), observations of glacial meltwater (hereafter named GMW) fractions from beneath Antarctic ice shelves have been notably absent. Therefore, most ice shelf models lack any direct observational validation. Here we present the first noble gas measurements made beneath an Antarctic ice shelf.

2. Data and Methods

To quantify the fraction and the spatial distribution of GMW below Filchner Ice Shelf (FIS), we collected the first sub-ice shelf helium and neon samples from six boreholes located on FIS (Figure 1), hot-water drilled by a team from British Antarctic Survey and the Alfred Wegener Institute in the framework of the *Filchner*

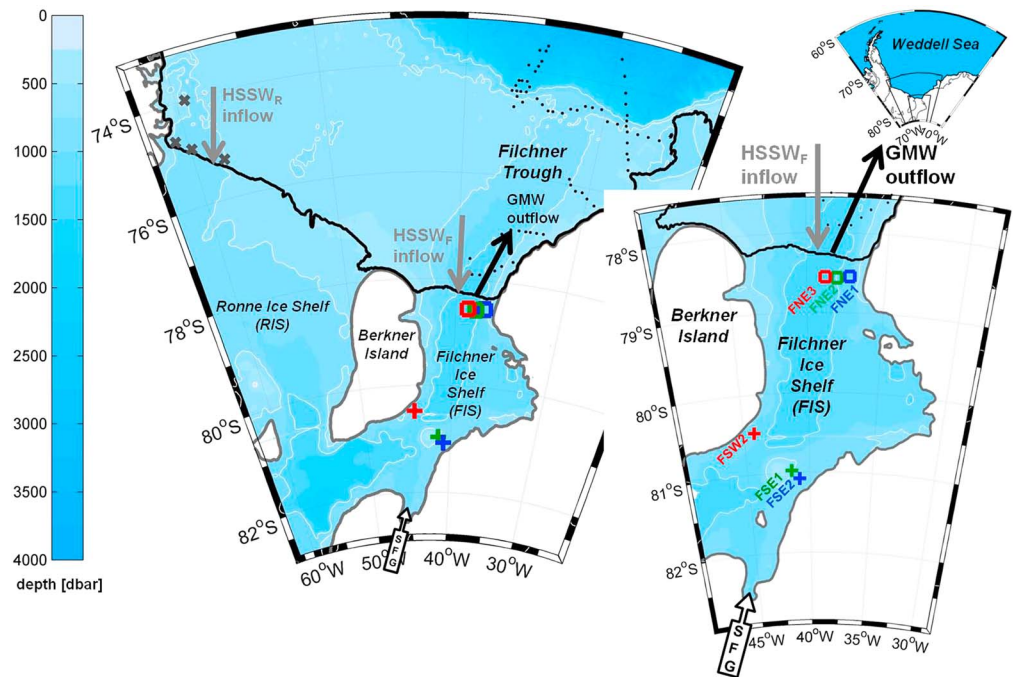


Figure 1. Map of the Filchner-Ronne Ice Shelf showing drill sites with noble gas data. Bold black line = ice shelf front; thick gray line = approximate grounding line; blue shading = isobaths in 250-m steps; thin white lines = 500- and 1,000-m isobaths. Berkner Island separates Ronne Ice Shelf (RIS) to the west from Filchner Ice Shelf (FIS). In the southeast, support force glacier (SFG) drains into FIS. Red, green, and blue crosses are the locations of the southern sites with noble gas data from 2015/2016. Red, green, and blue squares are the northern sites from 2016/2017. Black dots north of FIS are noble gas stations from 2014 (POLARSTERN cruise ANT29/9), gray crosses in front of RIS are noble gas stations from 1995 (ANT12/3). Gray and black arrows indicate the inflow of High Salinity Shelf Water (HSSW, subscript F and R denoting FIS and RIS inflow) and the outflow of glacial meltwater (GMW).

Ice Shelf Project (FISP) and the *Filchner Ice Shelf System (FISS)*. The samples were obtained using a newly developed gas-tight in situ water sampler (for details of sampling and later analysis, see Supporting Information S1). Three sites at around 81°S between Berkner Island and the mainland were occupied in 2015/2016 and are representative of the part of the ice shelf cavity where inflow from the Ronne Ice Shelf (RIS) determines the water column structure (Nicholls et al., 2009). Three sites around 78.5°S were sampled in 2016/2017. As they are located only ~50–65 km south of the FIS ice front, they could potentially be influenced by water masses formed north of the ice shelf (Figure 1). The FIS cavity samples (Huhn, Hattermann, et al., 2017) are supplemented by oceanic noble gas samples in front of FIS and RIS (Figure 1; Huhn, Rhein, et al., 2017; Roether & Huhn, 2017).

The stable noble gases helium and neon are weakly soluble in seawater and, therefore, are present in low concentrations. Away from sources and sinks, He and Ne are found to be in excess of their atmospheric equilibrium concentration by 3–4% throughout the water column (Huhn et al., 2008; Well & Roether, 2003). These supersaturations are caused mainly by air injection into the mixed layer by submerged air bubbles. If a significant He and Ne excess is found simultaneous, that excess can only be caused by subglacial melting (Schlosser, 1986; Schlosser et al., 1990).

Glacial ice traps atmospheric air during the snow-firn-ice transformation, slightly modifying the noble gas isotopic ratio (Loose & Jenkins, 2014). When the meteoric ice melts at the base of an ice shelf, the enhanced hydrostatic pressure causes the noble gases trapped in the air bubbles to dissolve fully in the water. This leads to a He concentration of 25.7 nmol/kg and a Ne concentration of 90.1 nmol/kg in pure GMW (Loose & Jenkins, 2014). This large excess provides an excellent tool to detect and quantify GMW fractions as low as 0.05% (Huhn et al., 2008; Schlosser, 1986; Sültenfuß et al., 2009).

Some GMW may be enriched in crustal He (i.e., the isotope ^4He) from α -decay of uranium and thorium and their daughter products in the bedrock beneath an ice sheet (crustal He-enriched subglacial runoff, SGR,

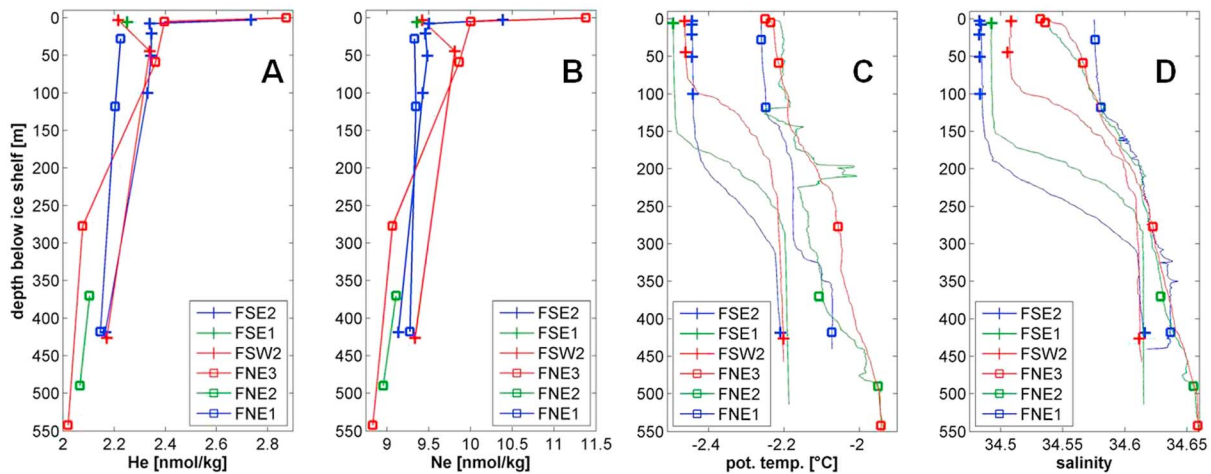


Figure 2. Helium, neon, mean temperature, and salinity profiles beneath the ice shelf base. Colors and symbols as in Figure 1. Helium (a) and neon (b) profiles from all six sites. Potential temperature (c) and salinity (d) are mean profiles from these sites. The uncertainty of the He and Ne concentrations is $\pm 0.5\%$. Zero meter is located at the base of the ice shelf, that is, ~ 750 dbar at the southern sites and ~ 530 dbar at the northern sites.

formed upstream or near the grounding line of the ice shelf). On geological timescales, the crustal He accumulate in the overlying ice up to 300 m above the bedrock (Beird et al., 2015; Bieri et al., 1964; Craig & Scarsi, 1997; Suess & Wänke, 1963). A He surplus of 4.5 ± 0.5 times that of GMW has been observed (Craig & Scarsi, 1997) in deep ice that has been near to bedrock. Other authors have reported a surplus He ratio in subglacial lake ice of 3.0 to 3.8 times that of GMW (Jean-Baptiste et al., 2001). The exact ratio depends on the composition of the bedrock and the time the ice or subglacial water has been in contact with it.

Some He (mainly primordial ^3He) is also added to the ocean's interior by hydrothermal activity (Clarke et al., 1969; Craig et al., 1975; Roether et al., 1998), whereas for Ne, the atmosphere is the only source.

3. Results

3.1. He and Ne Distribution Below FIS

At the southern sites (FSW2, FSE1, and FSE2), the He and Ne samples were primarily taken from two hydrographically well-mixed zones, the upper 100–200 m below the ice shelf base and in the 200–250 m thick layer above the bottom (Figures 2a and 2b). The potential temperatures (θ) close to the ice shelf base is low (-2.44 °C to 2.49 °C, Figure 2c) but still slightly warmer than the in situ freezing temperatures (i.e., at the pressure of the FIS base at each site; Figure SI.3 in the supporting information). At all sites, the bottom layer is warmer and more saline (mean θ and S profiles in Figures 2c and 2d; the individual profiles are in Figure SI.2 and θ/S in Figure SI.3 in the supporting information).

The hydrographic conditions at the northern sites (FNE1–FNE3) are more complex, and the He and Ne samples were collected throughout the water column. Compared with the southern sites, θ near the ice shelf base is higher (-2.2 to -2.25 °C). The in situ freezing point at the northern ice shelf base at ~ 530 dbar is -2.3 °C. As in the case of the southern sites, temperature and salinities increase with depth, and near-bottom salinities are similar at all the sites.

He and Ne concentrations (Figures 2a and 2b) close to the ice shelf base are generally higher than those deeper in the cavity, which we attribute to gas enrichment from local or nearby basal melting. Even in the cavity's deepest layers, however, the noble gas concentrations far exceed the equilibrium values of ocean surface waters or the ambient water found in front of the FRIS, indicating that GMW is present throughout the entire water column. The vertical density stratification at all sites suggests that the presence of GMW is unlikely to be the result of local vertical mixing. Instead, the deep GMW signal must be sourced through advection from below the RIS farther upstream (Ice Shelf Water with θ less than the surface freezing temperature due to basal meltwater admixtures was observed south of Berkner Island previously; Nicholls et al., 2001), or through accumulation due to recirculating water within the entire FRIS cavity.

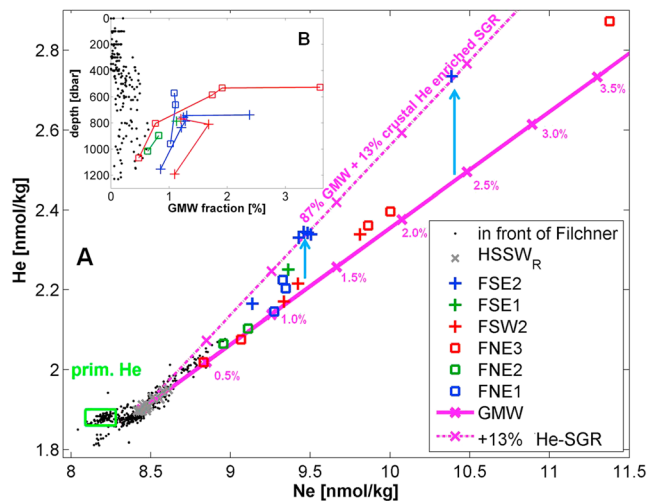


Figure 3. A Ne versus He and Figure 3b calculated glacial meltwater (GMW) fractions below Filchner Ice Shelf (FIS) and in front of FIS. Data colors and symbols as in Figure 1. Panel (a) shows the correlation between He and Ne. Solid magenta line indicates mixing of High Salinity Shelf Water flowing into the Ronne Ice Shelf cavity in the west (gray crosses; HSSW_R, observed maximum salinity of 34.87 with He = 1.90 nmol/kg and Ne = 8.44 nmol/kg) with pure GMW (Ne = 90.1 nmol/kg; He = 25.7 nmol/kg). The magenta marks on the GMW line indicate GMW fraction every 0.5%. He concentrations above the GMW mixing line indicate addition of crustal He accumulated in the ice from α -decay from the underlying bedrock. The dashed magenta line represents a mixing line between HSSW_R and a combination of 87% GMW plus 13% crustal He-enriched subglacial runoff (SGR) with He 4.5 times higher than in GMW. The green rectangle highlights data at the shelf break and slope with primordial He. Panel (b) shows the calculated GMW fractions based on Ne.

The highest He and Ne concentrations are found directly beneath the ice shelf base at FNE3 and FSE2 (the latter is closest to Support Force Glacier, SFG in Figure 1). The high concentrations near the ice shelf base at FNE3 can be explained by the absence of a mixed layer (Figures 2c and 2d), the noble gases are not diluted by mixing over the upper 100–150 m of the water column, so that the increase in He and Ne toward the ice shelf base is mirrored by the decrease in θ and S .

At FSE2, the water column in the upper 150 m is well mixed with respect to θ and S (Figures 2c and 2d), but not with respect to He and Ne in the uppermost sample (Figures 2a and 2b). Our hypothesis is that this sample 3 m below the ice shelf base is subject to refreezing, which would explain why we do not observe a salinity decrease (see also section 3.3 and Figure 4). Contamination with air during sampling can be ruled out, since the He/Ne ratio clearly points to addition of crustal He as in the samples below (see section 3.2 and the dashed magenta line in Figure 3a; contamination with air would follow a line parallel to the solid magenta line). The $^3\text{He}/^4\text{He}$ ratio (not shown) also support the addition of crustal He instead of atmospheric air. Furthermore, ice platelets below the ice shelf base were observed with a camera, also pointing to refreezing nearby.

At FSW2 (Figures 2a and 2b), the maximum noble gas signal was found 44 m below the ice shelf base. As the uppermost sample at this site was obtained 80 min prior to the samples below, the difference is likely related to the strong tidal variability beneath FIS that can substantially alter the water column structure over an individual tidal cycle (supporting information Figure SI.2 for FSW2, casts 23 vs. 24; and Figure SI.4, red crosses for FSW2).

3.2. GMW Fractions From He and Ne and Crustal He Addition

GMW fractions (Figure 3b) are quantified using the observed relationship between the He and Ne concentrations (Figure 3a) measured below the ice shelf and in front of FIS (Figure 1).

Most of the samples follow the mixing line toward pure GMW (solid magenta line, Figure 3a), with higher fractions at the base of FIS and smaller fractions deeper in the water column (Figure 3b). GMW fractions of up to 3.6% were observed close to the ice shelf base at FNE3 (red squares, Figures 3a and 3b). Even 500 m below FIS (below 1,000 dbar), the GMW fractions remain above 0.5%. GMW fractions in front of FIS are smaller than 0.6% but still significant (black dots, Figures 3a and 3b) and the maximum is located at \sim 800 dbar (Figure 3b), which is deeper than the GMW maximum at the southern (\sim 750 dbar) and northern (\sim 530 dbar) boreholes. Surface samples in front of FIS show only small GMW fractions ($<$ 0.2%), either due to dilution with ambient water or because of He and Ne equilibration with the atmosphere.

A distinct He surplus of 0.1 and 0.2 nmol/kg above the GMW mixing line (solid magenta line, Figure 3a) was found at the southeasternmost site at FSE2 (blue crosses and light blue arrows, Figure 3a), indicating the addition of crustal He from α -decay in the bedrock into the lower level of the ice stream and into SGR. Indeed, potential temperature-salinity properties show that increased He concentrations at FSE2 are associated with a deviation from the *Gade line* (Gade, 1979, 1993) toward a less saline mixing line (supporting information Figure SI.3) that cannot be explained by local ice shelf melting, but would be expected from such a freshwater source upstream or near the grounding line. A possible explanation is He-enriched injection of SGR from Support Force Glacier (SFG in Figure 1). Support Force Glacier is one of the principal glaciers feeding FIS and is the nearest ice stream (180 km) that could be the source for this locally focused crustal He-enriched SGR addition. Assuming He is 4.5 times higher in SGR than in GMW (Beaird et al., 2015; Craig & Scarsi, 1997), roughly 13% of the total meltwater observed at FSE2 consists of SGR (dashed magenta line, Figure 3a).

Some of the samples with the lowest Ne concentrations in front of FIS (black dots highlighted by the green square, Figure 3a) show somewhat higher helium concentrations compared with the GMW mixing line. This signal, observed between 500 and 1,000 dbar at the continental shelf break and slope at the northern end of

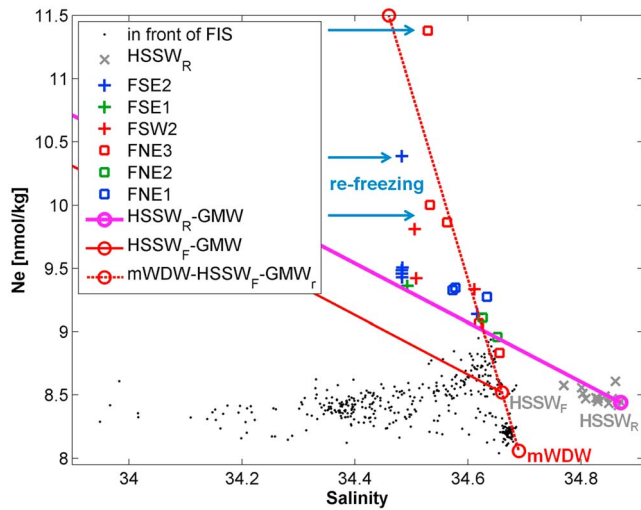


Figure 4. Ne versus salinity. Data colors and symbols as in Figure 1. The solid magenta line denotes the mixing of pure glacial meltwater (GMW; $S = 0$, $Ne = 90.1$ nmol/kg) and High Salinity Shelf Water (HSSW) formed in front of Ronne Ice Shelf (HSSW_R, gray crosses; $S \sim 34.88$ and $Ne \sim 8.47$ nmol/kg) that enters the Filchner-Ronne Ice Shelf (FRIS) cavity in the west. The light blue arrows to the right of that line indicate refreezing. Alternatively, the solid red line represents mixing between pure GMW and HSSW found in front of Filchner Ice Shelf, FIS (HSSW_F, $S = 34.66$ and $Ne = 8.52$ nmol/kg). The dashed red line indicates mixing between partly refrozen GMW (GMW_r), HSSW_F and modified warm deep water (mWDW), observed at the shelf break in front of the Filchner trough ($S = 34.69$, $\theta = +0.7$ °C, $Ne = 8.06$ nmol/kg, 500–1,000 dbar, see Figure 3a, data in the green rectangle).

the Filchner Trough, is much smaller than the He anomaly observed at the boreholes and results from hydrothermal sources outside the Weddell Sea (Well et al., 2003). If the signal were a remnant of GMW from beneath FRIS, the samples would be expected to show a small Ne anomaly and lie along the GMW mixing line. The hydrothermal source for this signal is further supported by the associated $^3\text{He}/^4\text{He}$ ratios (not shown).

The FRIS cavity is flushed by cold shelf water (High Salinity Shelf Water, HSSW, Figure 1), resulting in relatively low melt rates. Ice shelves in contact with warmer water originating from the Antarctic Circumpolar Current are expected to yield more GMW (Biddle et al., 2017; Heywood et al., 2016; Kim et al., 2016). However, noble gas-based observations of GMW fractions below other ice shelves are not available, and comparisons are only possible with observations from near their ice fronts. For example, the Dotson and Getz Ice Shelves in the Amundsen Sea exhibit far higher melt rates than beneath FRIS (Paolo et al., 2015; Rignot et al., 2013). In the Dotson Trough, maximum GMW fractions of $\sim 1\%$ at 400–500 dbar and He concentrations up to 2.4 nmol/kg have been observed, with GMW fractions increasing to 2% at ~ 170 dbar directly in front of the Dotson Glacier (Kim et al., 2016). In contrast, we found GMW fractions in front of FIS to be up to 0.6% GMW at ~ 800 dbar. Thus, in the Dotson and Getz cavities there is reason to believe that GMW fractions are likely far higher than those observed inside the FIS cavity.

3.3. Refreezing Fractions

The relationship between noble gas measurements and salinity allow us to infer rates of refreezing (Figure 4). HSSW formed during sea ice formation in front of RIS (Ronne High Salinity Shelf Water, HSSW_R; the gray crosses in

Figure 4) enters the FRIS cavity in the west (Nicholls et al., 2009; indicated by the left gray arrow in Figure 1), circulates within the cavity and fuels melting at the ice shelf base. This is indicated by the mixing line between HSSW_R and pure GMW (solid magenta line, Figure 4). Most of the sub-ice shelf samples from the southern sites (crosses, Figure 4) follow this line.

As water below the ice shelf refreezes, salt remains in the liquid phase leaving water masses with a higher salinity (Schlosser, 1986) than that expected from the meltwater mixing line (to the right of the solid magenta line in Figure 4). Several samples from the upper layers at the southern sites (FSW2 and FSE2) and more from the northern sites close to the FIS front—especially FNE3—show higher than expected salinities (light blue arrows in Figure 4). Refreezing fractions of about 0.8% to 2.7% (FNE3, red squares vs. solid magenta line in Figure 4) would produce the observed Ne/salinity relations. FNE3 is the borehole closest to an area of the northern FIS where extensive basal freezing is known to occur (Grosfeld et al., 1998; Rignot et al., 2013).

The HSSW observed in front of FIS (HSSW_F) is less saline than that in front of RIS (Figure 4). If the cavity at the northern sites is influenced by the slightly fresher HSSW_F, the calculated refreezing fractions would increase to 3.2% (FNE3, red squares vs. solid red line).

The samples that clearly show refreezing (GMW_r, particularly those from FNE3) are located near a mixing line that has HSSW_F as an end member. If this mixing line is extended toward higher salinities, it intersects the characteristics of modified Warm Deep Water (mWDW, dashed red line in Figure 4), as it is observed at the continental shelf break and on the slope in front of the Filchner Trough (data inside the green rectangle in Figure 3). The mWDW is a Weddell Sea variety of one of the main water masses of the Antarctic Circumpolar Current. Model results suggest that significant quantities of mWDW may penetrate into the FIS cavity in the future, drastically increasing basal melting (Hellmer et al., 2012; Timmermann & Hellmer, 2013). However, the intrusion of mWDW from the deep Weddell Sea and slope onto the shelf or even into the FRIS cavity at present can only be suggested by our data and must be subject to further investigations.

3.4. Basal Melt Rates

The mean GMW fraction beneath FIS deduced from our noble gas samples is $1.3 \pm 0.7\%$. The volume of the Filchner-Ronne cavity is $\sim 136,200$ Gt freshwater (R. Timmermann, personal communication, November 22, 2017). If we assume that it takes 10 years to completely exchange all water inside the cavity (exchange times between 5 and 14 years can be found in the literature; Gammelsrød et al., 1993; Mensch et al., 1996; Nicholls & Østerhus, 2004), this suggests that the mean melt rate beneath FRIS is 177 ± 95 Gt/year. This independent estimate confirms previous results for the FRIS that are based on modeled surface mass balance and remote sensing observations of ice flow velocities and ice shelf thickness changes (Ronne: 113.5 ± 35 Gt/year; Filchner: 41.9 ± 10 Gt/year; sum: 155.4 ± 36 Gt/year; Rignot et al., 2013). Furthermore, it agrees with the estimate of $4.3 \text{ m}^3/\text{s}$ (or 136 Gt/year), based on previous He observations (Schlosser et al., 1990).

The observations beneath FIS are snapshots from two different years. In such a short period of time, significant changes in melting and melt rates beneath FRIS are likely small; hence, the southern (2015/2016) and northern (2016/2017) noble gas data and the derived GMW fractions are comparable with each other. This is also supported by the similar He, Ne, and GMW values in the deeper part of the cavity (Figures 3band SI.4 in the supporting information). More critical, however, may be the time difference between the data in front of RIS, which were used to determine the properties of the inflowing HSSW_R end member. These data were obtained more than 20 years prior to the cavity measurements. Melt rate variability on this time scale could be substantial (Paolo et al., 2015), altering the end member He and Ne values and changing the slope of the mixing line. Resampling noble gas concentrations in this location should be a priority.

4. Summary and Conclusion

This study presents the first quantitative assessment of GMW fractions beneath an Antarctic ice shelf based on helium and neon samples obtained with a novel in situ gas-tight water sampler, deployed through hot-water-drilled boreholes. It provides an innovative view on the three-dimensional spatial variability of GMW inside the FIS cavity. The unique He and Ne measurements show the presence of GMW throughout the FIS cavity (0.5–3.6%; Figures 3a and 3b). At one site a distinct local addition of crustal He-enriched SGR (13% of the total meltwater) is identified, revealed by a significant higher He/Ne ratio (Figure 3a). Refreezing fractions of 0.8–2.7% are also observed (Figure 4). Our results provide a benchmark against which ice shelf cavity conditions in models investigating the interaction between the ocean and ice shelves can be compared.

Acknowledgments

We like to thank the Alfred Wegener Institute (AWI) and the British Antarctic Survey (BAS) for supporting the FISP (<https://www.awi.de/en/science/climate-sciences/physical-oceanography/projects/fisp.html>) and FISS (<https://www.bas.ac.uk/project/fiss/>) drilling campaigns 2015/2016 and 2016/2017 by logistics and funding. We acknowledge the work of Gerhard Fraas, who designed an early version of a noble-gas in situ water sampler. O. Huhn acknowledges funding by the Deutsche Forschungsgemeinschaft (DFG, SPP 1158 "Antarktisforschung", grants HU 1544/2 and HU 1544/4). The used data are archived and can be retrieved from Pangaea: <https://doi.pangaea.de/10.1594/PANGAEA.883808> (FIS ice shelf cavity, 2015/2016 and 2016/2017), <https://doi.pangaea.de/10.1594/PANGAEA.883799> (ANT29/9, 2013/2014), <https://doi.pangaea.de/10.1594/PANGAEA.883832> (ANT 12/3, 1995).

References

- Aeschbach, W. (2016). New perspectives for noble gases in oceanography. *Journal of Geophysical Research: Oceans*, 121, 6550–6554. <https://doi.org/10.1002/2016JC012133>
- Bamber, J. L., Riva, R. E. M., Vermeersen, B. L. A., & LeBrocq, A. M. (2009). Reassessment of the potential sea-level rise from a collapse of the West Antarctic ice sheet. *Science*, 324(5929), 901–903. <https://doi.org/10.1126/science.1169335>
- Baird, N., Straneo, F., & Jenkins, W. (2015). Spreading of Greenland meltwaters in the ocean revealed by noble gases. *Geophysical Research Letters*, 42, 7705–7713. <https://doi.org/10.1002/2015GL065003>
- Biddle, L. C., Heywood, K. J., Kaiser, J., & Jenkins, A. (2017). Glacial meltwater identification in the Amundsen Sea. *Journal of Physical Oceanography*, 47, 933–954. <https://doi.org/10.1175/JPO-D-16-0221.1>
- Bieri, R., Koide, M., & Goldberg, E. D. (1964). Noble gases in sea water. *Science*, 146(3647), 1035–1037. <https://doi.org/10.1126/science.146.3647.1035>
- Clarke, W. B., Beg, M. A., & Craig, H. (1969). Excess ^3He in the sea: Evidence for terrestrial primordial helium. *Earth and Planetary Science Letters*, 6(3), 213–220. [https://doi.org/10.1016/0012-821X\(69\)90093-4](https://doi.org/10.1016/0012-821X(69)90093-4)
- Corr, H. F. J., Jenkins, A., Nicholls, K. W., & Doake, C. S. M. (2002). Precise measurement of changes in ice-shelf thickness by phase-sensitive radar to determine basal melt rates. *Geophysical Research Letters*, 29(8), 1232. <https://doi.org/10.1029/2001GL014618>
- Craig, H., Clarke, W. B., & Beg, M. A. (1975). Excess ^3He in deep water on the East Pacific rise. *Earth and Planetary Science Letters*, 26(2), 125–132. [https://doi.org/10.1016/0012-821X\(75\)90079-5](https://doi.org/10.1016/0012-821X(75)90079-5)
- Craig, H., & Scarsi, P. (1997). Helium isotope stratigraphy in the GISP2 ice core. *Eos, Transactions American Geophysical Union*, 78(7).
- Foldvik, A., Gammelsrød, T., & Tørresen, T. (1985). *Circulation and water masses on the southern Weddell Sea shelf* (pp. 5–20). Washington, DC: American Geophysical Union. <https://doi.org/10.1029/AR043p0005>
- Gade, H. G. (1979). Melting of ice in sea water: A primitive model with application to the Antarctic ice shelf and icebergs. *Journal of Physical Oceanography*, 9(1), 189–198. [https://doi.org/10.1175/1520-0485\(1979\)009<0189:MOIISW>2.0.CO;2](https://doi.org/10.1175/1520-0485(1979)009<0189:MOIISW>2.0.CO;2)
- Gade, H. G. (1993). When ice melts in sea water: A review. *Atmosphere-Ocean*, 31(1), 139–165. <https://doi.org/10.1080/07055900.1993.9649466>
- Gammelsrød, T., Foldvik, A., Nøst, O. A., Foldvik, Ø., Anderson, L. G., Fogelqvist, E., et al. (1993). *Distribution of water masses on the continental shelf in the southern Weddell Sea* (pp. 159–176). Washington, DC: American Geophysical Union. <https://doi.org/10.1029/GM085p0159>
- Grosfeld, K., Hellmer, H. H., Jonas, M., Sandhäger, H., Schulte, M., & Vaughan, D. G. (1998). *Marine ice beneath Filchner ice shelf: Evidence from a multi-disciplinary approach* (pp. 319–339). Washington, DC: American Geophysical Union. <https://doi.org/10.1029/AR075p0319>
- Hellmer, H. H. (2004). Impact of Antarctic ice shelf basal melting on sea ice and deep ocean properties. *Geophysical Research Letters*, 31, L10307. <https://doi.org/10.1029/2004GL019506>

- Hellmer, H. H., Kauker, F., Timmermann, R., Determann, J., & Rae, J. (2012). Twenty-first-century warming of a large Antarctic ice-shelf cavity by a redirected coastal current. *Nature*, *485*(7397), 225–228. <https://doi.org/10.1038/nature11064>
- Heywood, K. J., Biddle, L. C., Boehme, L., Dutrieux, P., Fedak, M., Jenkins, A., et al. (2016). Between the devil and the deep blue sea: The role of the Amundsen Sea continental shelf in exchanges between ocean and ice shelves. *The Oceanography Society*, *29*(4), 118–129. <https://doi.org/10.2307/24862287>
- Hohmann, R., Schlosser, P., Jacobs, S., Ludin, A., & Weppernig, R. (2002). Excess helium and neon in the Southeast Pacific: Tracers for glacial meltwater. *Journal of Geophysical Research*, *107*(C11), 3198. <https://doi.org/10.1029/2000JC000378>
- Huhn, O., Hattermann, T., Davis, P., Dunker, E., Hellmer, H. H., Nicholls, K. W., et al. (2017). Filchner Ice Shelf cavity noble gas (helium and neon) measurements. <https://doi.pangaea.de/10.1594/PANGAEA.883808>
- Huhn, O., Rhein, M., Rodehacke, C., Roether, W., & Schodlok, M. P. (2008). Evidence of deep- and bottom-water formation in the western Weddell Sea. *Deep Sea Research Part II: Topical Studies in Oceanography*, *55*(8–9), 1098–1116. <https://doi.org/10.1016/j.dsr2.2007.12.015>
- Huhn, O., Rhein, M., Schröder, M., Bulsiewicz, K., & Sültenfuß, J. (2017). CFC, and noble gas measurements during POLARSTERN cruise PS82 (ANT-XXIX/9). <https://doi.pangaea.de/10.1594/PANGAEA.883799>
- Jacobs, S. S., Jenkins, A., Giulivi, C. F., & Dutrieux, P. (2011). Stronger ocean circulation and increased melting under Pine Island glacier ice shelf. <https://doi.org/10.1038/NGEO1188>
- Jean-Baptiste, P., Petit, J., Lipenkov, V. Y., Raynaud, D., & Barkov, N. I. (2001). Constraints on hydrothermal processes and water exchange in Lake Vostok from helium isotopes. *Nature*, *411*(6836), 460–462. <https://doi.org/10.1038/35078045>
- Kim, I., Hahm, D., Rhee, T. S., Kim, T. W., Kim, C. S., & Lee, S. H. (2016). The distribution of glacial meltwater in the Amundsen Sea, Antarctica, revealed by dissolved helium and neon. *Journal of Geophysical Research: Oceans*, *121*, 1654–1666. <https://doi.org/10.1002/2015JC011211>
- Loose, B., & Jenkins, W. J. (2014). The five stable noble gases are sensitive unambiguous tracers of glacial meltwater. *Geophysical Research Letters*, *41*, 2835–2841. <https://doi.org/10.1002/2013GL058804>
- Mensch, M., Bayer, R., Bullister, J. L., Schlosser, P., & Weiss, R. F. (1996). The distribution of tritium and CFCs in the Weddell Sea during the mid-1980s. *Progress in Oceanography*, *38*(4), 377–415. [https://doi.org/10.1016/S0079-6611\(97\)00007-4](https://doi.org/10.1016/S0079-6611(97)00007-4)
- Nicholls, K. W., Abrahamsen, E. P., Buck, J. J. H., Dodd, P. A., Goldblatt, C., Griffiths, G., et al. (2006). Measurements beneath an Antarctic ice shelf using an autonomous underwater vehicle. *Geophysical Research Letters*, *33*, L08612. <https://doi.org/10.1029/2006GL025998>
- Nicholls, K. W., & Makinson, K. (1998). *Ocean circulation beneath the western Ronne Ice Shelf, as derived from in situ measurements of water currents and properties* (pp. 301–318). Washington, DC: American Geophysical Union. <https://doi.org/10.1029/AR075p0301>
- Nicholls, K. W., & Østerhus, S. (2004). Interannual variability and ventilation timescales in the ocean cavity beneath Filchner-Ronne Ice Shelf, Antarctica. *Journal of Geophysical Research*, *109*, C04014. <https://doi.org/10.1029/2003JC002149>
- Nicholls, K. W., Østerhus, S., Makinson, K., Gammelsrød, T., & Fährbach, E. (2009). Ice-ocean processes over the continental shelf of the southern Weddell Sea, Antarctica: A review. *Reviews of Geophysics*, *47*, RG3003. <https://doi.org/10.1029/2007RG000250>
- Nicholls, K. W., Østerhus, S., Makinson, K., & Johnson, M. R. (2001). Oceanographic conditions south of Berkner Island, beneath Filchner-Ronne ice shelf, Antarctica. *Journal of Geophysical Research*, *106*(C6), 11,481–11,492. <https://doi.org/10.1029/2000JC000350>
- Paolo, F. S., Fricker, H. A., & Padman, L. (2015). Volume loss from Antarctic ice shelves is accelerating. *Science*, *348*(6232), 327–331. <https://doi.org/10.1126/science.aaa0940>
- Rignot, E., Jacobs, S., Mouginito, J., & Scheuchl, B. (2013). Ice-shelf melting around Antarctica. *Science*, *341*(6143), 266–270. <https://doi.org/10.1126/science.1235798>
- Roether, W., & Huhn, O. (2017). Chlorofluorocarbons, noble gases and tritium measurements during POLARSTERN cruise ANT-XXII/3 - Filchner-Ronne Ice Shelf. <https://doi.pangaea.de/10.1594/PANGAEA.883832>
- Roether, W., Well, R., Putzka, A., & Rütth, C. (1998). Component separation of oceanic helium. *Journal of Geophysical Research*, *103*(C12), 27,931–27,946. <https://doi.org/10.1029/98JC02234>
- Schlosser, P. (1986). Helium: A new tracer in Antarctic oceanography. *Nature*, *321*(6067), 233–235. <https://doi.org/10.1038/321233a0>
- Schlosser, P., Bayer, R., Foldvik, A., Gammelsrød, T., Rohardt, G., & Münnich, K. O. (1990). Oxygen 18 and helium as tracers of ice shelf water and water/ice interaction in the Weddell Sea. *Journal of Geophysical Research*, *95*(C3), 3253. <https://doi.org/10.1029/JC095iC03p03253>
- Schodlok, M. P., Menemenlis, D., & Rignot, E. J. (2016). Ice shelf basal melt rates around Antarctica from simulations and observations. *Journal of Geophysical Research: Oceans*, *121*, 1085–1109. <https://doi.org/10.1002/2015JC011117>
- Shepherd, A., Ivins, E., Rignot, E., Smith, B., van den Broeke, M., Velicogna, I., et al. (2018). Mass balance of the Antarctic ice sheet from 1992 to 2017. *Nature*, *558*(7709), 219–222. <https://doi.org/10.1038/s41586-018-0179-y>
- Shepherd, A., Ivins, E. R., Geruo, A., Barletta, V. R., Bentley, M. J., Bettadpur, S., et al. (2012). A reconciled estimate of ice-sheet mass balance. *Science*, *338*(6111), 1183–1189.
- Suess, H. E., & Wänke, H. (1963). On the possibility of a helium flux through the ocean floor. *Progress in Oceanography*, *3*, 347–353. [https://doi.org/10.1016/0079-6611\(65\)90030-3](https://doi.org/10.1016/0079-6611(65)90030-3)
- Sültenfuß, J., Roether, W., & Rhein, M. (2009). The Bremen mass spectrometric facility for the measurement of helium isotopes, neon, and tritium in water. *Isotopes in Environmental and Health Studies*, *45*(2), 83–95. <https://doi.org/10.1080/10256010902871929>
- Timmermann, R., & Hellmer, H. H. (2013). Southern Ocean warming and increased ice shelf basal melting in the twenty-first and twenty-second centuries based on coupled ice-ocean finite-element modelling. *Ocean Dynamics*, *63*(9–10), 1011–1026. <https://doi.org/10.1007/s10236-013-0642-0>
- Well, R., & Roether, W. (2003). Neon distribution in South Atlantic and South Pacific waters. *Deep Sea Research Part I: Oceanographic Research Papers*, *50*(6), 721–735. [https://doi.org/10.1016/S0967-0637\(03\)00058-X](https://doi.org/10.1016/S0967-0637(03)00058-X)
- Well, R., Roether, W., & Stevens, D. P. (2003). An additional deep-water mass in Drake Passage as revealed by 3He data. *Deep Sea Research Part I: Oceanographic Research Papers*, *50*(9), 1079–1098. [https://doi.org/10.1016/S0967-0637\(03\)00050-5](https://doi.org/10.1016/S0967-0637(03)00050-5)
- Weppernig, R., Schlosser, P., Khatiwala, S., & Fairbanks, R. G. (1996). Isotope data from Ice Station Weddell: Implications for deep water formation in the Weddell Sea. *Journal of Geophysical Research*, *101*(C11), 25,723–25,739. <https://doi.org/10.1029/96JC01895>